



A fully divergence-free method for generation of inhomogeneous and anisotropic turbulence with large spatial variation

Rixin Yu*, Xue-Song Bai

Division of Fluid Mechanics, Lund University, 221 00 Lund, Sweden

ARTICLE INFO

Article history:

Received 1 March 2013

Received in revised form 14 June 2013

Accepted 27 August 2013

Available online 6 September 2013

Keywords:

Inflow generation method

Inhomogeneous and anisotropic turbulence

Large spatial variation

Divergence-free

DNS

LES

ABSTRACT

A fully divergence-free method is proposed for generation of inhomogeneous/anisotropic turbulence with large spatial variation. The method is based on the method of Smirnov et al., which is known to violate the divergence-free constraint when spatial variation of turbulence is present. In the proposed method a vector potential field is introduced; by taking the vector curl of the potential field one can generate a strictly divergence-free flow field. A novel formulation for scaling the vector potential field, together with a coordinate transformation strategy, is proposed in this work. The result is a six-step procedure for the generation of inhomogeneous turbulence fields. The proposed formulation is proven to reproduce the prescribed velocity correlation with energy spectrum at large Reynolds numbers. Four test cases are considered to evaluate the new method. First, the statistical quantities introduced in the proposed method are verified numerically in a classical homogeneous turbulence case. Then, the performance of the new method is demonstrated in three different inhomogeneous turbulence cases: a confined turbulent flow in a “slip-wall” box, a planar channel flow and an annular flow. It is shown that the unphysical patterns in the fluctuation fields and divergence errors produced with Smirnov's method are absent in the results from the new method. The accuracy of the proposed methods is verified by comparing the velocity correlations with the prescribed scaling functions. The proposed method is efficient and simple to implement.

© 2013 Elsevier Inc. All rights reserved.

1. Introduction

Specification of initial and inflow boundary conditions for direct numerical simulation or large eddy simulation of turbulent flows is an important issue that can affect the accuracy of the simulations [1,2]. There are two major categories of methods for generation of initial or inflow conditions: precursor simulation and synthetic turbulence. The precursor method relies on data from a genuine turbulence simulation; detailed reviews and discussions on this method can be found in Refs. [3,4]. In the synthetic approach the turbulence field is generated by certain algorithms accommodating randomness. There are three often-used types of the method: the spectral method [5,6], the digital filter method [7–9] and the synthesis eddy method (SEM) [10]. The last two are more recent ones. In the digital filter method the inflow generation is achieved through filtering the random data to satisfy a prescribed second order statistics and correlation function [7]. In the SEM method turbulence is viewed as a superposition of coherent structures and the method is implemented as synthesizing eddies represented by specific shape functions [10]. The spectrum method works in the wave space. Kraichnan [5] was the

* Corresponding author.

E-mail address: rixin.yu@energy.lth.se (R. Yu).

first to propose synthesizing Fourier waves for homogeneous turbulence. The method was further extended by Smirnov et al. [6] and Batten et al. [11] to account for general inhomogeneous and anisotropic turbulence. The spectrum methods by Kraichnan and Smirnov are simple and have been implemented into commercial software.

One important requirement for the synthesizing turbulence method is that the results should satisfy the divergence-free (also known as solenoidal) property for an incompressible flow. While emphasizing on producing physical statistics or coherence, both the original digital filter method and SEM method do not satisfy the divergence-free constraint. For the SEM method this issue is investigated in a recent work [12] based on using a vorticity field and solving of a Poisson equation. The obvious advantage of the spectrum method is that the divergence-free property is satisfied under homogeneous conditions, since the continuity equation is satisfied for each individual wave vector in the Kraichnan method. To extend the method for general inhomogeneous and anisotropic turbulence, Smirnov proposed a framework consisting of a scaling step and an orthogonal transformation step. The process is based on Cholesky decomposition of the local Reynolds stress tensor. As pointed out in [6], while the solenoidal property is not affected by the orthogonal transformation step, the scaling step can result in a velocity field that is not divergence-free. In Smirnov's method the scaling coefficient is assumed to be a slowly varying function and its gradient is negligible, therefore the method yields an "essentially" divergence-free field. This assumption, however, may not be applicable under the general inhomogeneous turbulence of engineering and academic interests. For example, rather significant spatial variations in inflow turbulence may exist in the shear layer of a jet or a wall boundary layer. This solenoidal issue was recently discussed by Huang et al. [13]. Instead of using the scaling step and the orthogonal transformation step, they propose a solution based on modifying the distribution strategy of the wave vector (\mathbf{k}) in Kraichnan's original method for homogeneous turbulence. This method is better in accounting for anisotropy, however, it is still difficult to account for the inhomogeneity caused by large spatial variation.

It is important to ensure the divergence-free constraint for the initial and inflow generation. Violation of the constraint can introduce a non-physical pattern into the simulation and hence affect the accuracy of the results. In previous works [7,8] it was suggested to use an extra projection step to remove the divergence error. In addition to increased algorithmic complexity the projection method has other drawbacks. Firstly, it can be problematic to define a unique projection operator over the entire domain; for example, boundary conditions, such as periodicity, are not necessarily satisfied in the non-projected field. Furthermore, a projection step will modify the flow field, which can result in an undefined deviation from the desired statistics (such as velocity correlations) prescribed for the non-projected field.

In this work we propose a new method that can be strictly divergence-free while still within the general Smirnov's framework of using a scaling step and an orthogonal transformation step. The idea is based on the observation that any divergence-free (solenoidal) vector field can be written as the vector curl of a vector potential field (a special case of Helmholtz theorem), and vice versa. Therefore, we propose to work with the vector potential field instead of on the velocity field. A modified scaling procedure will then be applied to the vector potential field, which can then be computed by a numerical approximation of the curl operator that can be easily constructed to generate a solenoidal velocity field. The proposed method can handle general inhomogeneity with rather significant spatial variation in the scaling coefficients; the method is simple to implement.

The structure of this paper is as follows: in Section 2 we will give a brief review of Smirnov's method, followed by a detailed description of the new method. Section 3 shows the required mathematical proof together with the derivation of the proposed formulation for scaling the vector potential field. In Section 4 the new method is verified using four test cases. The first case is for homogeneous turbulence in which most of the relations involved in the proof are verified numerically. We then demonstrate the new method in three inhomogeneous turbulence cases having academic or practical relevance.

2. Method descriptions

The method proposed in this work is based on the Random Flow Generation (RFG) method of Smirnov et al. [6] for generating an inhomogeneous and anisotropic turbulent flow field \mathbf{u} . Before presenting the new method, it is useful to give a brief overview of the original method.

2.1. Overview of Smirnov's method

The Smirnov method is made up of the following three steps:

Step 1. For an anisotropic velocity correlation tensor r_{ij} of a turbulent flow field \mathbf{u} ,

$$r_{ij} = \langle u_i u_j \rangle, \quad (1)$$

where $\langle \rangle$ stands for the ensemble averaging, the first step is to find an orthogonal tensor a_{ij} to diagonalize r_{ij} ,

$$a_{mi} r_{ij} a_{nj} = c_{(n)}^2 \delta_{mn}. \quad (2)$$

The diagonal coefficients c_n are the square roots of the eigenvalues corresponding to the real symmetrical matrix r_{ij} . Here, variables in bold letter stand for the vector form. In the tensor form, following Ref. [6], repeated sub-indexes means summation while parentheses around indexes avoids summation.

Step 2. The second step is a modified Kraichnan method, written for a transient flow field \mathbf{v} as:

$$\mathbf{v}(\mathbf{x}, t) = \sum_{n=1}^{N_T} [\mathbf{p}^n \cos(\tilde{\mathbf{k}}^n \cdot \mathbf{x} + \omega^n t) + \mathbf{q}^n \sin(\tilde{\mathbf{k}}^n \cdot \mathbf{x} + \omega^n t)], \quad (3)$$

where

$$\tilde{k}_j^n = k_j^n \frac{L/\tau}{c_{(j)}}, \quad (4)$$

and

$$\mathbf{p}^n = \boldsymbol{\zeta}^n \times \mathbf{k}^n, \quad \mathbf{q}^n = \boldsymbol{\xi}^n \times \mathbf{k}^n. \quad (5)$$

In the above formulations L and τ are turbulence length and time scales respectively. The two vectors $\boldsymbol{\zeta}$ and $\boldsymbol{\xi}$ were selected randomly from a Gaussian distribution. N_T is the total number of randomly picked waves with frequencies ω^n and wave-number vector \mathbf{k}^n ; they are randomly distributed to satisfy statistical isotropy and a realizable energy spectrum. The main difference between the Smirnov method and the Kraichnan method lies in the use of a modified $\tilde{\mathbf{k}}$ instead of \mathbf{k} .

Step 3. \mathbf{v} is scaled to an intermediate velocity field \mathbf{w} and then further orthogonally transformed to the final flow field \mathbf{u} ,

$$w_i = c_{(i)} v_{(i)}, \quad (6)$$

$$u_i = a_{ij} w_j. \quad (7)$$

It is known that the orthogonal transformation, Eq. (7), preserves the solenoidal property if \mathbf{w} is divergence-free.

2.2. Non-zero divergence in Smirnov's method

Note that in the above Step 3 the \mathbf{c} -scaling is directly applied upon \mathbf{v} to generate \mathbf{w} , which can cause non-zero divergence of \mathbf{w} when the scaling field \mathbf{c} is not divergence-free:

$$\partial w_i / \partial x_i = v_i \partial c_i / \partial x_i + c_i \partial v_i / \partial x_i. \quad (8)$$

In Ref. [6] the second term on the right-hand side (r.h.s.) of the above equation is argued to be zero according to the following relation,

$$c_i \partial v_i / \partial x_i = \tau \sqrt{2/N_T} \sum_{n=1}^{N_T} \left[-p_i^n k_i^n \sin\left(\frac{l/\tau}{c_j(\mathbf{x})} k_{(j)}^n \frac{x_{(j)}}{l}\right) + q_i^n k_i^n \cos\left(\frac{l/\tau}{c_j(\mathbf{x})} k_{(j)}^n \frac{x_{(j)}}{l}\right) \right] = 0. \quad (9)$$

We should point out here that for the above argument to be correct the following relation needs to be satisfied,

$$\frac{\partial}{\partial x_i} \left(\frac{k_{(j)}}{c_j(\mathbf{x})} x_{(j)} \right) = \frac{k_{(j)}}{c_j(\mathbf{x})} \delta_{ij}. \quad (10)$$

This, however, cannot be strictly true if $c_j(\mathbf{x})$ is non-uniformly distributed in space.

Smirnov argued that the first term on the r.h.s. of Eq. (8) can be neglected if \mathbf{c} is assumed to be slowly varying with \mathbf{x} and its derivative is small. Together with Eq. (9), \mathbf{w} will then be approximately divergence-free. However, for general cases there may exist rather large spatial variation of \mathbf{c} , such as in the near wall boundary region. In such cases the inhomogeneous flow field generated with Smirnov's method may contain non-negligible divergence error, which can introduce uncertainty to the numerical simulations. In the following section we propose a new method to overcome this issue.

2.3. The new method

Note that any solenoidal vector field (\mathbf{V}) can always be expressed as the vector curl of a vector potential field (\mathbf{A}) (a special case of Helmholtz decomposition),

$$\nabla \times \mathbf{A} = \mathbf{V}, \quad (11)$$

$$\nabla \cdot \mathbf{V} = \nabla \cdot (\nabla \times \mathbf{A}) = 0. \quad (12)$$

Instead of working on the velocity field, we propose here to work on the vector potential of the velocity field. We first generate a vector potential (Ψ) corresponding to the homogeneous flow field (\mathbf{v}); then, we modify it to Φ with a new scaling formulation and another coordinate transformation operation. The modified vector potential can then be taken curl to calculate the scaled flow field (\mathbf{w}) to be strictly divergence-free.

Step 1. Cholesky decomposition of local Reynolds stress

This step is the same as step 1 of Simonov's method in which the scaling coefficients (c_j) and the orthogonal transformation tensor a_{ij} are computed.

Step 2. Coordinate transformation

Assume that the flow field is defined on \mathbf{x} -coordinate within a box domain of size $D_1^X \times D_2^X \times D_3^X$, with $x_i \in [0, D_i^X]$ for $i = 1, 2, 3$. Introduce a coordinate transformation function ($\bar{c}_i(\mathbf{x})$), which is only a function of x_i ,

$$\partial \bar{c}_i / \partial x_j = 0, \quad \forall i \neq j. \quad (13)$$

Using \bar{c}_i , a new coordinate \mathbf{y} is constructed from \mathbf{x} as:

$$y_i(x_i) = \int_{x'=0}^{x_i} \bar{c}_i(x')^{-1} \cdot dx'. \quad (14)$$

The Jacobian matrix of the coordinate transformation ($J_{ij} = \partial y_i / \partial x_j$) becomes:

$$J_{ij}(x_1, x_2, x_3) = \begin{bmatrix} \bar{c}_1(x_1)^{-1} & 0 & 0 \\ 0 & \bar{c}_2(x_2)^{-1} & 0 \\ 0 & 0 & \bar{c}_3(x_3)^{-1} \end{bmatrix}. \quad (15)$$

Step 3. The homogeneous vector potential

Generate a vector potential field on the \mathbf{y} coordinate, $\Psi(\mathbf{y}, t)$, corresponding to the homogeneous flow field (\mathbf{v})

$$\mathbf{v} = \nabla \times \Psi, \quad (16)$$

in a domain of size $D_1^Y \times D_2^Y \times D_3^Y$ ($D_i^Y = y_i(D_i^X)$). Rewrite the Kraichnan method using the Fourier series as:

$$\Psi(\mathbf{y}, t) = \sum_{n=1}^{N_T} [\hat{\Psi}(\mathbf{k}^n) \exp(i\mathbf{k}^n \cdot \mathbf{y} + \omega^n t) + \hat{\Psi}^*(\mathbf{k}^n) \exp(-i\mathbf{k}^n \cdot \mathbf{y} + \omega^n t)], \quad (17)$$

where $i^2 = -1$ and $\hat{\Psi}$ is the complex-valued mode vector and the superscript star denotes complex conjugate. A total of N_T number of wave-number vectors (\mathbf{k}^n) can be selected from a random distribution as in Refs. [5,6]. In this work we set N_T as the total number of discretely available \mathbf{k}^n . For example, on a uniform grid of $N_1 \times N_2 \times N_3$ cells any \mathbf{k}^n can be written as:

$$k_i^n = 2\pi m_i / D_{(i)}^Y \quad (18)$$

with the integer number vector (\mathbf{m}) given by

$$m_i \in [0, N_i/2] \quad \text{and} \quad m_1 > 0 \cup (m_1 = 0) \cap (m_2 > 0 \cup (m_2 = 0 \cap m_3 > 0)). \quad (19)$$

$\hat{\Psi}$ is set as:

$$\hat{\Psi}(\mathbf{k}^n) = (D_1^Y D_2^Y D_3^Y)^{-1/2} \sqrt{\frac{E(k/2\pi)}{2\pi(k/2\pi)^2}} \frac{\mathbf{z}^n}{|\mathbf{z}^n \times \mathbf{k}^n|}, \quad (20)$$

where $k = |\mathbf{k}^n|$. The energy spectrum $E(\kappa)$ is defined on the spectroscopic wave number $\kappa = k/2\pi$. \mathbf{z}^n is a non-zero complex vector; the real part of the \mathbf{z} is generated by (For convenience the superscript n is omitted):

$$\text{Re}(\mathbf{z})/m_{\mathfrak{R}} = \cos \varphi_{\mathfrak{R}} \frac{\cos \theta_{\mathfrak{R}} \cdot (\mathbf{n} \times \mathbf{k}) / |\mathbf{n} \times \mathbf{k}| + \sin \theta_{\mathfrak{R}} \cdot \mathbf{n} / |\mathbf{n}|}{|\cos \theta_{\mathfrak{R}} \cdot (\mathbf{n} \times \mathbf{k}) / |\mathbf{n} \times \mathbf{k}| + \sin \theta_{\mathfrak{R}} \cdot \mathbf{n} / |\mathbf{n}||} + \sin \varphi_{\mathfrak{R}} \frac{\mathbf{k}}{|\mathbf{k}|}. \quad (21)$$

The imaginary part of the vector ($\text{Im}(\mathbf{z})$) is similarly generated except replacing the subscript \mathfrak{R} with \mathfrak{I} . In the above formulation \mathbf{n} is an arbitrarily chosen real vector perpendicular to \mathbf{k} , i.e., $\mathbf{n} \cdot \mathbf{k} = 0$; $\theta_{\mathfrak{R}}$ and $\theta_{\mathfrak{I}}$ are two random angles uniformly distributed in $[-\pi, \pi]$; $\varphi_{\mathfrak{R}}$ and $\varphi_{\mathfrak{I}}$ are two random angles uniformly distributed in $[-\varphi^R, \varphi^R]$ with $0 \leq \varphi^R < \pi/2$; $m_{\mathfrak{R}}$ and $m_{\mathfrak{I}}$ are two real random value within $(0, 1]$.

With Ψ given by Eq. (17) and from Eq. (16), the homogeneous flow field (\mathbf{v}) can be written as:

$$\mathbf{v}(\mathbf{y}, t) = \sum_{n=1}^{N_T} (\hat{\mathbf{v}}(\mathbf{k}^n) \exp(i\mathbf{k}^n \cdot \mathbf{y} + \omega^n t) + \hat{\mathbf{v}}^*(\mathbf{k}^n) \exp(-i\mathbf{k}^n \cdot \mathbf{y} + \omega^n t)), \quad (22)$$

where the velocity mode vector ($\hat{\mathbf{v}}$) is:

$$\hat{\mathbf{v}}(\mathbf{k}^n) = \iota \mathbf{k}^n \times \hat{\Psi}(\mathbf{k}^n) = \iota (D_1^Y D_2^Y D_3^Y)^{-1/2} \sqrt{\frac{E(k/2\pi)}{2\pi(k/2\pi)^2}} \frac{\mathbf{k}^n \times \mathbf{z}^n}{|\mathbf{z}^n \times \mathbf{k}^n|}. \quad (23)$$

The above method for \mathbf{v} is a special case of Kraichnan's original approach. Although removed from the \mathbf{k}^n -selection strategy, the randomness is still retained in generating \mathbf{z}^n . Using the maximum N_T , one can now specify any energy spectrum $E(\kappa)$. In this work we test the following two spectra:

$$E_1(\kappa; U', L) = 16(2/\pi)^{1/2} U'^2 \kappa^4 L^5 \exp(-2\kappa^2 L^2), \quad (24)$$

$$E_2(\kappa; U', L, \text{Re}_L) = \frac{9}{4} \left(\frac{U'}{L} \right)^{\frac{2}{3}} \kappa^{-\frac{5}{3}} \left(\frac{\kappa L}{\sqrt{\kappa^2 L^2 + c_L}} \right)^{\frac{11}{3}} \exp\{-5.2\{\kappa^4 L^4 \text{Re}_L^{-3} + c_\eta^4\}^{\frac{1}{4}} - c_\eta\}. \quad (25)$$

Here, U' is the root mean square (rms) velocity component; L is the turbulent integral scale and $\text{Re}_L = \sqrt{\frac{3}{2}} U' L / \nu$ is the integral-scale Reynolds number, ν is the kinematic viscosity. The integration of any $E(\kappa)$ should be the turbulent kinetic energy, i.e.:

$$\int_{\kappa=0}^{\infty} E(\kappa) \cdot d\kappa = \frac{3}{2} U'^2. \quad (26)$$

In E_2 (Chapter 6.53 in Pope's book [14]) the constants c_L and c_η are calculated by both satisfying Eq. (26) and requiring the integration of $2\nu\kappa^2 E_2(\kappa)$ to be the turbulent dissipation rate ε . The first spectrum (E_1) is for relatively lower Reynolds number, which was also used in previous works [5,6]. The second spectrum (E_2) can cover a wide range of Reynolds number; it is used in this work to provide a comparable spectrum at higher Reynolds numbers. In the above relations the summation can be performed with the efficient Fast Fourier Transform (FFT) algorithm.

For homogeneous/isotropic turbulence, $\langle v_i v_i \rangle$ can be first written as integration of $\langle \hat{v}_i \hat{v}_i^* \rangle$ over the wave number vector space then reduced to integration of $E(\kappa)$ using Eq. (23); it finally recovers the $3U'^2$ term using Eq. (26):

$$\begin{aligned} \langle v_i v_i \rangle &= \frac{1}{D_1^Y D_2^Y D_3^Y} \iiint_{\mathbf{y}} \langle v_i(\mathbf{y}) v_i(\mathbf{y}) \rangle d\mathbf{y} = 2 \sum_{n=1}^{N_T} \langle \hat{v}_i(\mathbf{k}^n) \hat{v}_i^*(\mathbf{k}^n) \rangle \\ &\approx \frac{D_1^Y D_2^Y D_3^Y}{(2\pi)^3} \iiint_{\mathbf{k}} \langle \hat{v}_i(\mathbf{k}) \hat{v}_i^*(\mathbf{k}) \rangle \cdot d\mathbf{k} = \frac{1}{8\pi^3} \int_{\kappa=0}^{\infty} \frac{E(k/2\pi)}{2\pi(k/2\pi)^2} \cdot 4\pi k^2 dk \\ &= \int_{\kappa=0}^{\infty} 2E(\kappa) \cdot d\kappa = 3U'^2. \end{aligned} \quad (27)$$

It should be pointed out that Ψ can also be generated based on any existing methods that can produce a homogeneous/isotropic and periodic \mathbf{v} field. Since it is always possible to obtain the velocity mode vector ($\hat{\mathbf{v}}$) from inverse Fourier transform, the corresponding mode of the vector potential ($\hat{\Psi}$) can be generated by inverting Eq. (23) (straightforward to derive):

$$\hat{\Psi} = \frac{\iota}{k^2} \left(\hat{\mathbf{v}} \times \mathbf{k} + \mathbf{k} \frac{|\hat{\mathbf{v}} \times \mathbf{k}|}{k \tan \vartheta} \right) \quad (28)$$

where ϑ is a random number in $(0, \pi)$.

Step 4. The inhomogeneous vector potential

A new inhomogeneous vector potential (Φ) on the \mathbf{x} -coordinate can be generated by multiplying the corresponding Ψ on the \mathbf{y} -coordinate with a scaling function f . (The time dependency is omitted in the formulation for simplicity):

$$\Phi_i(\mathbf{x}) = \Psi_i(\mathbf{y}(\mathbf{x})) f_{(i)}(\mathbf{x}), \quad (29)$$

with

$$f_i(\mathbf{x}) = \frac{\bar{c}_1 \bar{c}_2 \bar{c}_3}{\bar{c}_i} \sqrt{\left(\frac{c_1^2}{\bar{c}_1^2} + \frac{c_2^2}{\bar{c}_2^2} + \frac{c_3^2}{\bar{c}_3^2} \right) - 2 \frac{c_{(i)}^2}{\bar{c}_{(i)}^2}}. \quad (30)$$

Step 5. The scaled velocity

The scaled velocity field (\mathbf{w}) is generated by taking the vector curl of Φ ,

$$\mathbf{w}(\mathbf{x}) = \nabla \times \Phi(\mathbf{x}). \quad (31)$$

In Section 3 it will be shown that under large Re_L numbers the correlation of this scaled new velocity can be approximated as:

$$\langle w_i w_j \rangle \approx U'^2 c_{(i)}^2 \delta_{ij}. \quad (32)$$

It is obvious that the scaled velocity (\mathbf{w}) from Eq. (31) is always divergence-free. In this work the derivative in the curl operator is discretized by a second order (and alternatively a fourth order) central difference scheme. For example on a collocated grid of integer indexing of (i, j, k) with uniform grid spacing of $(\Delta x_1, \Delta x_2, \Delta x_3)$, the 2nd order discrete curl for computing w_1 can be written:

$$\left(w_1 = \frac{\partial \Phi_2}{\partial x_3} - \frac{\partial \Phi_3}{\partial x_2} \right)_{i,j,k} = \frac{\Phi_{2;i,j,k+1} - \Phi_{2;i,j,k-1}}{2\Delta x_3} - \frac{\Phi_{3;i,j+1,k} - \Phi_{3;i,j-1,k}}{2\Delta x_2} + O(\Delta x_2^2) + O(\Delta x_3^2). \quad (33)$$

Step 6. Orthogonal transformations

Similar to step 3 of Smirnov's method, the final velocity (\mathbf{u}) is generated by applying orthogonal transformations onto the scaled velocity field (\mathbf{w}). The final turbulent flow field (\mathbf{u}) is divergence-free.

2.4. Comments on the new method

The coordinate transformation function (\bar{c}_i) and the new coordinate (\mathbf{y})

To avoid complex-valued f_i in Eq. (30), a general guideline of selecting \bar{c}_i is to satisfy,

$$\left(\frac{c_1^2}{\bar{c}_1^2} + \frac{c_2^2}{\bar{c}_2^2} + \frac{c_3^2}{\bar{c}_3^2} \right) - 2 \frac{c_{(i)}^2}{\bar{c}_{(i)}^2} \geq 0, \quad (34)$$

for all three i -directions over the entire \mathbf{x} -domain. As will be demonstrated in Section 4, it is not difficult to satisfy the above criterion for some typical \mathbf{c} configurations. However, for arbitrary \mathbf{c} configurations it is possible for this criterion to fail in certain regions of the \mathbf{x} -domain. In such cases, instead of using Eq. (30) we may locally set $f_i = 0$ in the affected i -direction. This only affects the local accuracy (causing deviation from the prescribed $\langle w_i w_j \rangle$), however, the final \mathbf{w} field remains divergence-free. If the spatial variation of c_i is small, \bar{c}_i can be simply set as the volume average of c_i over the entire domain. In such a case the new coordinate \mathbf{y} is chosen as,

$$y_i = \frac{x_i}{\bar{c}_{(i)}}. \quad (35)$$

For a homogeneous but anisotropic turbulence field (c_i is constant in space but different for each direction i), simply setting $\bar{c}_i = c_i$ with Eq. (35) results in similar scaling in wave number as that by Smirnov (Eqs. (3) and (4)), which also reduces Eq. (29) to,

$$\Phi_i(\mathbf{x}) = \Psi_i(\mathbf{y}) \frac{c_1 c_2 c_3}{c_{(i)}}. \quad (36)$$

The present method then becomes identical to the Smirnov method.

For a general choice of \bar{c}_i that can vary along x_i , the new coordinate \mathbf{y} should be generated using Eq. (14), which is clearly different from the Smirnov's scaling. Using FFT it is more convenient to generate Ψ on a uniformly spaced \mathbf{y} -grid, which then corresponds to a non-uniform \mathbf{x} -grid for a general \bar{c}_i . If the scaled velocity \mathbf{w} is required on a uniform \mathbf{x} -grid, it is convenient to first interpolate Ψ to the targeted uniform \mathbf{x} -grid and then calculate Φ and \mathbf{w} using a simple discrete curl operator on the uniform grid. This is, however, not necessary. Other types of grid (structured/unstructured) can be used for \mathbf{w} calculation, as long as the discretely curl operator can be constructed with reasonable accuracy.

It can be noted that multiplying an arbitrary constant number (Λ) with a coordinate transfer function $\bar{c}_a(\mathbf{x})$ satisfying criterion (34) can create a new function $\bar{c}_b(\mathbf{x}) = \Lambda \cdot \bar{c}_a(\mathbf{x})$ that also satisfies the criterion, which leads to a rescaling of the homogeneous domain size ($D_i^Y|_{\bar{c}_b} = \Lambda \cdot D_i^Y|_{\bar{c}_a}$). Unlike in Smirnov's method where a uniform integral scale L is "problematically" used for the inhomogeneous \mathbf{x} -domain, in the proposed method L is defined on the homogeneous \mathbf{y} -domain. It is clear that the above Λ -scaling is equivalent to varying the relative integral scale L/D_i^Y .

Algorithm complexity and efficiency. Compared with the Smirnov method, the proposed method requires two additional steps: a coordinate transformation step with potentially an interpolation procedure, and the calculation of the discrete vector curl. These two steps are simple to implement and fast to compute.

3. Derivation and proof

In this section we will show the proposed formulation for the new vector potential (Φ , Eq. (29) and (30)) can result in a scaled velocity (\mathbf{w}) with a properly scaled correlation tensor (Eq. (32)) under large Reynolds number.

Problem description. Using Eqs. (31), (29), (15) and the Levi-Civita symbol (ε_{ijk}), the scaled velocity \mathbf{w} can be split into two parts:

$$w_i = \tilde{w}_i + w'_i, \quad (37)$$

with

$$\tilde{w}_i = \varepsilon_{ijk} f_j \bar{c}_k^{-1} \frac{\partial \Psi_j}{\partial y_k}, \quad (38)$$

$$w'_i = \varepsilon_{ijk} \Psi_j \frac{\partial f_j}{\partial x_k}, \quad (39)$$

and

$$\langle w_i w_j \rangle = \langle \tilde{w}_i \tilde{w}_j \rangle + (\langle \tilde{w}_i w'_j \rangle + \langle \tilde{w}_j w'_i \rangle + \langle w'_i w'_j \rangle). \quad (40)$$

In the following (after Lemma 1) we will firstly show that by choosing f_j as Eq. (30), the correlation of first part, $\tilde{\mathbf{w}}$, can be written as:

$$\langle \tilde{w}_i \tilde{w}_j \rangle = U'^2 c_{(i)}^2 \delta_{ij}. \quad (41)$$

We will then show that under large Reynolds numbers – even in the presence of strong spatial variation, the other three statistics involving the second part \mathbf{w}' on the r.h.s. of Eq. (40) are negligible compared with $\langle \tilde{w}_i \tilde{w}_j \rangle$, therefore the total correlation $\langle w_i w_j \rangle$ can be estimated by Eq. (32).

Lemma 1. Consider a homogeneous/isotropic turbulence field (\mathbf{v}) with zero mean velocity and a rms velocity of U' ,

$$\langle v_i \rangle = 0, \quad (42)$$

$$\langle v_i v_j \rangle = U'^2 \delta_{ij}, \quad (43)$$

with a randomly generated vector potential Ψ satisfying Eq. (16) and

$$\langle \Psi_i \rangle = 0. \quad (44)$$

The following two relations hold:

$$\left\langle \frac{\partial \Psi_i}{\partial y_j} \Psi_k \right\rangle = 0, \quad (45)$$

$$\left\langle \frac{\partial \Psi_i}{\partial y_j} \frac{\partial \Psi_{(i)}}{\partial y_k} \right\rangle = \left\langle \frac{\partial \Psi_i}{\partial y_j} \frac{\partial \Psi_k}{\partial y_{(j)}} \right\rangle = \left\langle \frac{\partial \Psi_i}{\partial y_j} \frac{\partial \Psi_k}{\partial y_{(i)}} \right\rangle = 0, \quad \forall i \neq j \neq k. \quad (46)$$

Furthermore, the following relation holds:

$$\langle \Psi_i \Psi_j \rangle = \Omega \delta_{ij}, \quad (47)$$

with Ω estimated as:

$$\Omega \approx C_\# \int_{\kappa=0}^{\infty} \frac{E(\kappa)}{\kappa^2} \cdot d\kappa \approx \frac{1}{\Theta(\text{Re}_L)} L^2 U'^2, \quad (48)$$

where $C_\#$ is a constant independent of the energy spectrum $E(\kappa)$; for any given energy spectrum $\Theta(\text{Re}_L)$ is a monotonically increasing function of Re_L .

Furthermore, if the following relation is satisfied:

$$\left\langle \frac{\partial \Psi_i}{\partial y_j} \frac{\partial \Psi_{(j)}}{\partial y_{(i)}} \right\rangle = 0, \quad \forall i \neq j, \quad (49)$$

then the following relation also holds

$$\left\langle \frac{\partial \Psi_i}{\partial y_j}^2 \right\rangle = \frac{1}{2} U'^2, \quad \forall i \neq j. \quad (50)$$

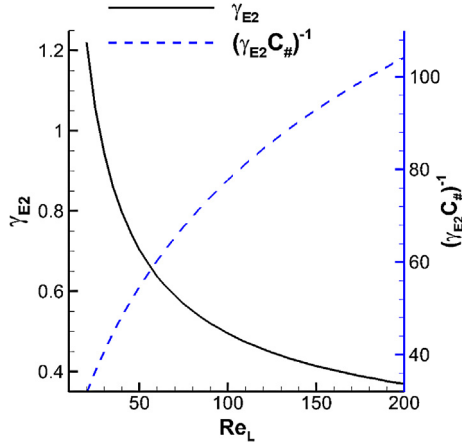


Fig. 1. γ_{E2} (Eq. (56)) and $(C_\# \gamma_{E2})^{-1}$ as a function of the Reynolds number Re_L . $C_\#$ is calculated using Eq. (53) with $\varphi^R = 0.315\pi$.

Proof. Assume that Ψ_i are three independent random sequences (white noise). Their spatial derivatives ($\frac{\partial \Psi_i}{\partial y_j}$) are related to the increment of white noise signal, which are still independent random sequences. Hence, Eqs. (45) and (46) are valid.

Using the isotropy assumption $\langle \Psi_i \Psi_j \rangle$ can be reduced to Eq. (47). For the homogeneous vector potential field generated using Eqs. (20) and (21), similar to the derivation of $\langle v_i v_i \rangle$ in Eq. (27), $\langle \Psi_i \Psi_i \rangle$ can be written as,

$$\frac{1}{3} \langle \Psi_i \Psi_i \rangle = \Omega = \frac{2}{3} \sum_{n=1}^{N_T} \langle \hat{\Psi}_i(\mathbf{k}^n) \hat{\Psi}_i^*(\mathbf{k}^n) \rangle \approx C_\# \int_{\kappa=0}^{\infty} \frac{E(\kappa)}{\kappa^2} d\kappa \quad (51)$$

where

$$C_\# = \frac{1}{6\pi^2} \left\langle \frac{|\text{Im}(\mathbf{z})|^2 + |\text{Re}(\mathbf{z})|^2}{|\text{Im}(\mathbf{z})|^2 \cos^2 \varphi_{\Re} + |\text{Re}(\mathbf{z})|^2 \cos^2 \varphi_{\Im}} \right\rangle, \quad (52)$$

which results in the first estimation of Ω in Eq. (48). For general selection of \mathbf{z} , it is simple to see $\frac{1}{6}\pi^{-2} \leq C_\# \leq \frac{1}{6}\pi^{-2} \cos^{-2} \varphi^R$. If $|\text{Im}(\mathbf{z})| = |\text{Re}(\mathbf{z})|$ (as being set in Section 4.1), $C_\#$ can be further simplified as:

$$C_\# = \frac{1}{6\pi^2} \langle \cos^{-2} \varphi_{\Re} \rangle = \frac{\tan \varphi^R}{6\pi^2 \varphi^R}. \quad (53)$$

For a chosen φ^R , Ω depends on the integration of $E(\kappa)/\kappa^2$ only. Using the simple spectrum E_1 , Ω can be analytically integrated as:

$$\Omega|_{E_1} \approx C_\# \cdot 2L^2 U'^2 = \frac{\tan \varphi^R}{3\pi^2 \varphi^R} L^2 U'^2. \quad (54)$$

For the more complicated spectrum E_2 , Ω becomes,

$$\Omega|_{E_2} \approx C_\# \cdot \gamma_{E_2}(Re_L) L^2 U'^2, \quad (55)$$

with

$$\gamma_{E_2}(Re_L) = \frac{9}{4} \int_{t=0}^{\infty} (t^2 + c_L)^{-11/6} \exp(-5.2[t^4 Re_L^{-3} + c_\eta^4]^{1/4} - c_\eta) dt. \quad (56)$$

Thus, $\Theta(Re_L)|_{E_2} = C_\#^{-1} \gamma_{E_2}^{-1}(Re_L)$. Using numerical integration, one can determine the functions $\gamma_{E_2}(Re_L)$ and $C_\#^{-1} \gamma_{E_2}^{-1}(Re_L)$. As shown in Fig. 1, $\Theta(Re_L)|_{E_2}$ is a monotonically increasing function of Re_L .

For general turbulent energy spectra other than E_1 or E_2 , it can be useful to estimate Ω based on a physical argument. Note that Ψ and \mathbf{v} are related to each other in a similar way to \mathbf{v} and the strain rate S , ($S = \sqrt{S_{ij}^2}$, $S_{ij} = (\partial v_i / \partial y_j + \partial v_j / \partial y_i)/2$), i.e. the latter is a spatial first derivative of the former. As such, Ω can be estimated following a dimensional analysis:

$$\frac{\Omega}{U'^2} \sim \frac{U'^2}{\langle S^2 \rangle} = \frac{U'^2}{\varepsilon/v} \sim \frac{U'^2}{(U'^3/L)/v}. \quad (57)$$

Rewriting Eq. (57) yields a heuristic estimation of Ω as Eq. (48) with $\Theta(\text{Re}_L) \sim \text{Re}_L$.

Eq. (50) can be obtained by expanding Eq. (16) for the $i = 1$ component,

$$U'^2 = \langle v_1 v_1 \rangle \equiv \left\langle \left(\frac{\partial \Psi_2}{\partial y_3} - \frac{\partial \Psi_3}{\partial y_2} \right)^2 \right\rangle = \left\langle \frac{\partial \Psi_2^2}{\partial y_3} \right\rangle + \left\langle \frac{\partial \Psi_3^2}{\partial y_2} \right\rangle - 2 \left\langle \frac{\partial \Psi_3}{\partial y_2} \frac{\partial \Psi_2}{\partial y_3} \right\rangle, \quad (58)$$

and using the isotropy assumption and Eq. (49).

The above relations in Lemma 1 (Eqs. (43), (45)–(48), (49) and (50)) will be further verified numerically in Section 4.1.

3.1. The $\langle \tilde{w}_i \tilde{w}_j \rangle$ term

$\tilde{\mathbf{w}}$ can be expanded as,

$$\begin{aligned} \tilde{w}_1 &= f_2 \bar{c}_3^{-1} \partial \Psi_2 / \partial y_3 - f_3 \bar{c}_2^{-1} \partial \Psi_3 / \partial y_2, \\ \tilde{w}_2 &= f_3 \bar{c}_1^{-1} \partial \Psi_3 / \partial y_1 - f_1 \bar{c}_3^{-1} \partial \Psi_1 / \partial y_3, \\ \tilde{w}_3 &= f_1 \bar{c}_2^{-1} \partial \Psi_1 / \partial y_2 - f_2 \bar{c}_1^{-1} \partial \Psi_2 / \partial y_1. \end{aligned} \quad (59)$$

Then $\langle \tilde{w}_i \tilde{w}_j \rangle$ can be determined using Eqs. (46), (49) and (50), by imposing Eq. (41):

$$\langle \tilde{w}_i \tilde{w}_j \rangle = \frac{1}{2} U'^2 \begin{bmatrix} f_2^2 \bar{c}_3^{-2} + f_3^2 \bar{c}_2^{-2} & 0 & 0 \\ 0 & f_1^2 \bar{c}_3^{-2} + f_3^2 \bar{c}_1^{-2} & 0 \\ 0 & 0 & f_1^2 \bar{c}_2^{-2} + f_2^2 \bar{c}_1^{-2} \end{bmatrix} = U'^2 \begin{bmatrix} c_1^2 & 0 & 0 \\ 0 & c_2^2 & 0 \\ 0 & 0 & c_3^2 \end{bmatrix}, \quad (60)$$

which leads to the following equation for \mathbf{f} ,

$$\begin{bmatrix} 0 & \bar{c}_3^{-2} & \bar{c}_2^{-2} \\ \bar{c}_3^{-2} & 0 & \bar{c}_1^{-2} \\ \bar{c}_2^{-2} & \bar{c}_1^{-2} & 0 \end{bmatrix} \begin{bmatrix} f_1^2 \\ f_2^2 \\ f_3^2 \end{bmatrix} = 2 \begin{bmatrix} c_1^2 \\ c_2^2 \\ c_3^2 \end{bmatrix}. \quad (61)$$

It is clear that Eq. (30) is the solution to the above equation. Since f_i is not allowed to be a complex number, Eq. (34) is required.

3.2. The remaining term

Using Eq. (45),

$$\langle \tilde{w}_i w'_j \rangle = 0. \quad (62)$$

From Eq. (47), one has

$$\langle w'_i w'_j \rangle = \varepsilon_{imn} \varepsilon_{jm' n'} \frac{\partial f_m}{\partial x_n} \frac{\partial f_m}{\partial x_{n'}} \Omega. \quad (63)$$

Since \mathbf{f} is a function of c_i as in Eq. (30), its spatial derivative is closely related to the spatial derivative of c_i . For an inhomogeneous field with reasonably large spatial variation in the local \mathbf{c} field, i.e.,

$$|\partial f_m / \partial x_n| \sim |\partial c_m / \partial x_n| < C_g / L, \quad \text{with } C_g \in [1/2, 10], \quad (64)$$

together with the estimations in Eqs. (48) and (64), $\langle w'_i w'_j \rangle$ can be estimated to be bounded,

$$\langle w'_i w'_j \rangle < U'^2 C_g^2 / \Theta(\text{Re}_L). \quad (65)$$

From Eqs. (62), (65) and (40), it is clear that Eq. (32) is valid at large Re_L numbers, even in the presence of strong spatial variation.

4. Results and discussion

Indicator of divergence-free error. In the following, we examine the divergence of the velocity field. A departure from divergence-free can be quantified using the following two error indicators, an absolute error (ε_{div}) or a relative error ($\varepsilon_{\text{div}}^R$), defined as

$$\varepsilon_{\text{div}}(\mathbf{u}) = |\partial u_1 / \partial x_1 + \partial u_2 / \partial x_2 + \partial u_3 / \partial x_3|, \quad (66)$$

$$\varepsilon_{\text{div}}^R(\mathbf{u}) = \frac{|\partial u_1 / \partial x_1 + \partial u_2 / \partial x_2 + \partial u_3 / \partial x_3|}{|\partial u_1 / \partial x_1| + |\partial u_2 / \partial x_2| + |\partial u_3 / \partial x_3| + \Delta e}, \quad (67)$$

where $\Delta e = 10^{-20}$ is added to avoid division by zero. Similar to the discrete curl operator (Eq. (33)), the corresponding second order or fourth order central difference scheme is used for discretization of the divergence operator on the discrete grid. In all the following examples of flow fields generated by the proposed method, the divergence-free property is verified by ensuring that $\varepsilon_{\text{div}}^R$ is always below 10^{-7} . In contrast, using Smirnov's method $\varepsilon_{\text{div}}^R$ at some locations can be close to 1. In the following discussions regarding Smirnov's method only the absolute error is considered.

Case description. The new method is first applied to generate homogeneous isotropic turbulence. For homogeneous turbulent flow the proposed method reduces to the original Kraichnan method. In this case, we will show both the flow and vector potential fields computed from single and multiple realizations. We will confirm numerically the statistical relations (43), (45), (46), (47), (48), (49) and (50) involved in Lemma 1, which is vital for estimating the accuracy of the new method when applied to the general inhomogeneous flows. To demonstrate the dependency of vector potential correlation on Reynolds number, Eq. (48), two energy spectra corresponding to low and high Reynolds numbers (e.g. E_1 and E_2 at $\text{Re}_L = 100$) are tested.

We will then apply the method to three cases of non-homogeneous flow with diagonal scaling coefficients resembling typical turbulent initial and inflow configurations, i.e. an artificial turbulence confinement by a “slip-wall” box (case 2), a turbulent planar channel flow (case 3), and a turbulent annular flow (case 4). In these cases different choices of \bar{c} are used and the criterion (34) is satisfied over the entire domain. It is trivial to show that the orthogonal transformation in step 6 does not affect solenoidal propriety; therefore, it will be excluded from the test examples. In each case, we will first compare the flow fields from a single realization of the present method and Smirnov's method with the E_1 spectrum. For comparison the transient flow field in Smirnov's method is generated using the same maximum N_T strategy as in Eq. (19). The spatial distribution of the error ε_{div} from Smirnov's method will be shown. In the proposed new method this error is zero. The velocity correlation tensor computed using the new method is examined and compared to the prescribed scaling functions.

In the following we consider the flow fields generated within a periodic rectangular \mathbf{x} -domain of size $D_1^X \times D_2^X \times D_3^X$, with a rms velocity $U' = 1$ m/s. The domain is discretized using a uniform grid of $N_1 \times N_2 \times N_3 = 256^3$ cells. The grid number is sufficient to support the spectrum with the chosen integral scale L in the homogeneous \mathbf{y} -domain. All the statistics are computed by ensemble averaging 1000 random realizations.

4.1. Homogeneous/isotropic turbulence

In this case the homogeneous/isotropic turbulence is generated in a cubic domain of side length $D_i^X = 4$ m ($i = 1, 2, 3$) and the turbulent integral scale $L = 1$ m. Following the procedure described in Section 2, we first generate the vector potential Ψ using Eqs. (17), (20) and (21), and then we compute the velocity \mathbf{v} by calculating the discrete curl with a 2nd order (and alternatively a 4th order) central difference scheme. For the implementation of Eq. (21) we set $\text{Im}(\mathbf{z}) = \text{Re}(\mathbf{z})$, namely, $\varphi_{\mathfrak{R}} = \varphi_{\mathfrak{I}}$, $\theta_{\mathfrak{R}} = \theta_{\mathfrak{I}}$ and $m_{\mathfrak{R}} = m_{\mathfrak{I}} = 1$, which has been found to accelerate the convergence of high-order statistics. It is found that the φ^R value for the distribution range of angle $\varphi_{\mathfrak{R}}$ and $\varphi_{\mathfrak{I}}$ can affect the value of $\langle \frac{\partial \Psi_i}{\partial y_j} \cdot \frac{\partial \Psi_{(j)}}{\partial y_{(i)}} \rangle$, $\forall i \neq j$ (the values of the different components are rather similar, as will be shown later). By setting $\varphi^R = 0.315\pi$ the left-hand side of Eq. (49) is approximately zero. For this reason, the above parameters are kept in the other cases as well. Since the above method is based on a special variant of Kraichnan's method, it is reasonable to expect that Eq. (49) is easier to be satisfied with a more general implementation of the random Ψ generation method.

Fig. 2 shows the fields of \mathbf{v} and Ψ from a single realization using the spectra E_1 and E_2 (at $\text{Re}_L = 100$). The flow field (\mathbf{v}_3 component and the velocity vector) with spectrum E_1 appears to be qualitatively similar to that reported in previous works [5,6]. Both spectra lead to rather homogeneously distributed structures in both the \mathbf{v}_3 and Ψ_2 fields. Compared with E_1 , the spectrum E_2 clearly produces much finer spatial scales in both the \mathbf{v} and Ψ fields. The fluctuation in the Ψ_2 field has a higher intensity with spectrum E_1 than with E_2 , implying a higher rms value of Ψ with E_1 . This is a direct consequence of Eq. (47) and (48).

Fig. 3 shows the spatial distribution of the correlation tensor $\langle \Psi_i \Psi_j \rangle$ with the spectrum E_1 . It is seen that the diagonal components ($\langle \Psi_1 \Psi_1 \rangle$ and $\langle \Psi_2 \Psi_2 \rangle$) oscillate around 0.05 ± 0.01 and the off-diagonal term ($\langle \Psi_1 \Psi_2 \rangle$) fluctuates around 0 ± 0.001 . The spatial fluctuations may be due to insufficient averaging samples and a slow convergence rate of second order moments. To reduce the random disturbances to the statistics quantities, we apply spatial-averaging to the present homogeneous turbulence case, written for any statistical field $\langle \phi \rangle$ as,

$$\langle \phi \rangle_V = \frac{1}{V} \iiint_V \langle \phi \rangle d\mathbf{v}, \quad (68)$$

where $d\mathbf{v}$ denotes the volume elements and V denotes the entire domain volume. Table 1 shows five spatially averaged quantities with the spectrum E_1 : $\langle v_i v_j \rangle$, $\langle \Psi_i \Psi_j \rangle$, $\langle \frac{\partial \Psi_i}{\partial y_j} \Psi_k \rangle$, $\langle \frac{\partial \Psi_i}{\partial y_j}^2 \rangle$, $\langle \frac{\partial \Psi_i}{\partial y_j} \frac{\partial \Psi_{(j)}}{\partial y_{(i)}} \rangle$ and a joint term representing the three terms involved in Eq. (46), $\langle \frac{\partial \Psi_i}{\partial y_j} \frac{\partial \Psi_{(i)}}{\partial y_k} \rangle$, $\langle \frac{\partial \Psi_i}{\partial y_j} \frac{\partial \Psi_k}{\partial y_{(j)}} \rangle$ and $\langle \frac{\partial \Psi_i}{\partial y_j} \frac{\partial \Psi_k}{\partial y_{(i)}} \rangle$, with the curl operator discretized using the 2nd order central difference scheme. The corresponding quantities with E_2 are shown in Table 2. (Being again small, the joint term is not

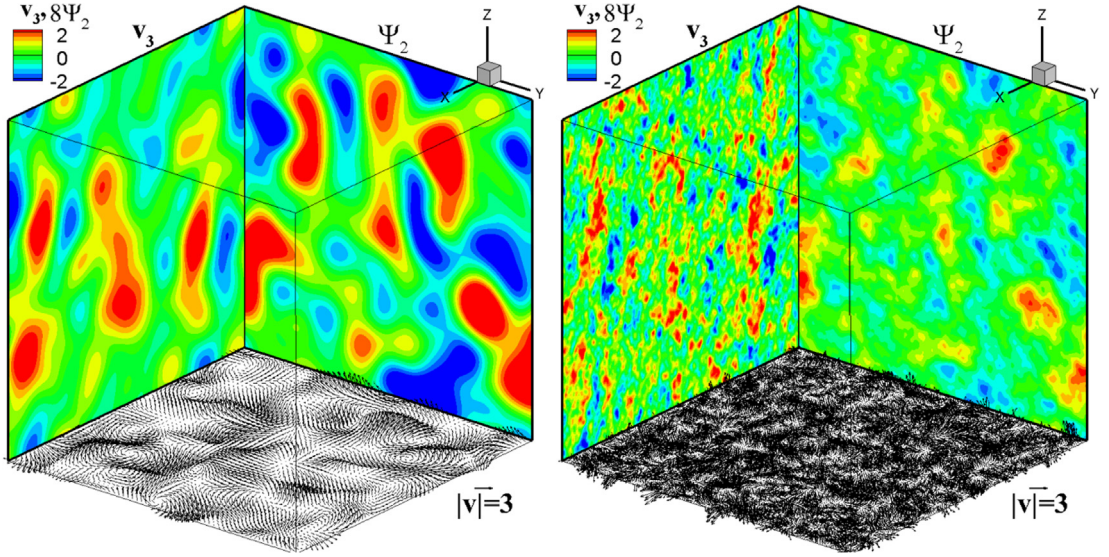


Fig. 2. A snap-shot of homogeneous/isotropic turbulent flow field (v_3 component and velocity vector plot) and the corresponding vector potential field (Ψ_2 component) generated using the low Reynolds number spectrum E_1 (left) and spectrum E_2 at $Re_L = 100$ (right), both with the integral scale $L = 1$ m.

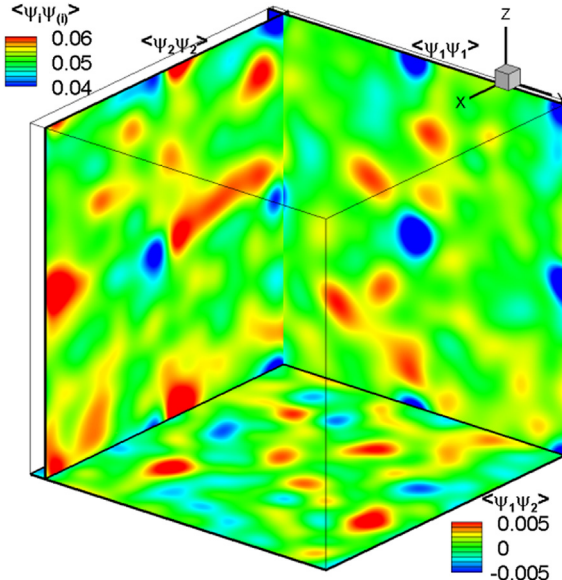


Fig. 3. Spatial distributions of the $\langle \psi_i \psi_j \rangle$ (i.e. $\langle \psi_1 \psi_1 \rangle$, $\langle \psi_2 \psi_2 \rangle$ and $\langle \psi_1 \psi_2 \rangle$), averaged from 1000 random realizations using spectrum E_1 .

shown here.) To show the effect of using higher order discrete curl operators, the diagonal terms of $\langle v_i v_j \rangle_V$ and $\langle \psi_i \psi_j \rangle_V$ for both spectra using the 4th order central difference scheme are shown in Table 3. With our variant of Kraichnan method for homogeneous/isotropic turbulence, it is clear that $\langle v_i v_j \rangle_V$ can recover the prescribed value of $U'^2 \delta_{ij}$, Eq. (43), for both spectra. The diagonal values of $\langle v_i v_j \rangle_V$ with E_2 are slightly less than unity (around 0.945/0.984 with the 2nd/4th order schemes respectively). This can be due to a combined effect of insufficient grid points to support the spectrum E_2 with integral scale $L = 1$ m ($256 \cdot L/D_i^Y = 64$ cells) and numerical integration errors introduced when determining the spectrum constants c_L and c_η in Eq. (25). The third order tensor $\langle \frac{\partial \Psi_i}{\partial y_j} \Psi_k \rangle_V$ using both spectra is essentially zero, which is consistent with Eq. (45) in Lemma 1. It is clear that Eq. (46) in Lemma 1 is satisfied, as shown by the joint term. $\langle \psi_i \psi_j \rangle_V$ appears to be a diagonal dominant tensor, a good approximation of $\Omega \delta_{ij}$ in Eq. (47) in Lemma 1. The values of Ω are different for the two spectra: for the lower Reynolds number spectrum E_1 they are around $5.15 \times 10^{-2}/4.97 \times 10^{-2}$ for the 2nd/4th order schemes respectively; while for the higher Reynolds number spectrum E_2 ($Re_L = 100$) the value is around $1.20 \times 10^{-2}/1.16 \times 10^{-2}$ for 2nd/4th order schemes respectively. The above Ω values are close to the theoretical values ($\Omega|_{E_1} = 5.20 \times 10^{-2}$ and $\Omega|_{E_2} = 1.29 \times 10^{-2}$) calculated by Eqs. (54) and (55) with $\varphi^R = 0.315\pi$. It is interesting to point

Table 1

Spatially-averaged statistical quantities of $\langle v_i v_j \rangle_V$, $\langle \Psi_i \Psi_j \rangle_V$, $\langle \frac{\partial \Psi_i}{\partial y_j} \Psi_k \rangle_V$, $\langle \frac{\partial \Psi_i}{\partial y_j}^2 \rangle_V$, $\langle \frac{\partial \Psi_i}{\partial y_j} \frac{\partial \Psi_{(j)}}{\partial y_{(i)}} \rangle_V$, and part of $\langle \frac{\partial \Psi_i}{\partial y_j} \frac{\partial \Psi_m}{\partial y_n} \rangle_V$ (respective unit: $m^2 s^{-2}$, $m^4 s^{-2}$, $m^3 s^{-2}$, $m^2 s^{-2}$ for the rest) computed from 1000 randomly generated homogeneous/isotropic turbulence fields using spectrum E_1 and the 2nd order central difference scheme. The last term represents a joint term by $\langle \frac{\partial \Psi_i}{\partial y_j} \frac{\partial \Psi_{(j)}}{\partial y_k} \rangle_V$, $\langle \frac{\partial \Psi_i}{\partial y_j} \frac{\partial \Psi_k}{\partial y_{(j)}} \rangle_V$ and $\langle \frac{\partial \Psi_i}{\partial y_j} \frac{\partial \Psi_k}{\partial y_{(i)}} \rangle_V$ in Eq. (46).

$\langle v_i v_j \rangle_V$	$j = 1$	$j = 2$	$j = 3$
$i = 1$	0.998	3.02×10^{-4}	-1.10×10^{-3}
$i = 2$	3.02×10^{-4}	0.997	-3.29×10^{-5}
$i = 3$	-1.10×10^{-3}	-3.29×10^{-5}	0.998
$\langle \Psi_i \Psi_j \rangle_V$	$j = 1$	$j = 2$	$j = 3$
$i = 1$	5.16×10^{-2}	-1.34×10^{-4}	-4.15×10^{-5}
$i = 2$	-1.34×10^{-4}	5.14×10^{-2}	-1.00×10^{-4}
$i = 3$	-4.15×10^{-5}	-1.00×10^{-4}	5.15×10^{-2}
$\langle \frac{\partial \Psi_i}{\partial y_j} \Psi_k \rangle_V$	$j = 1$	$j = 2$	$j = 3$
$i = 1, k = 1$	2.8×10^{-22}	1.0×10^{-17}	-2.3×10^{-17}
$i = 2, k = 1$	1.7×10^{-17}	1.8×10^{-21}	-4.8×10^{-18}
$i = 3, k = 1$	1.1×10^{-17}	-3.0×10^{-18}	-8.8×10^{-22}
$i = 1, k = 2$	-1.1×10^{-19}	-3.1×10^{-18}	8.6×10^{-18}
$i = 2, k = 2$	6.8×10^{-18}	-2.1×10^{-19}	2.8×10^{-17}
$i = 3, k = 2$	1.5×10^{-17}	-1.6×10^{-17}	6.4×10^{-20}
$i = 1, k = 3$	-1.1×10^{-18}	-2.3×10^{-17}	-3.8×10^{-18}
$i = 2, k = 3$	-2.0×10^{-18}	1.8×10^{-18}	1.4×10^{-18}
$i = 3, k = 3$	3.5×10^{-18}	2.0×10^{-17}	-2.8×10^{-17}
$\langle \frac{\partial \Psi_i}{\partial y_j}^2 \rangle_V$	$j = 1$	$j = 2$	$j = 3$
$i = 1$	×	0.5065	0.5059
$i = 2$	0.5046	×	0.5077
$i = 3$	0.5068	0.5049	×
$\langle \frac{\partial \Psi_i}{\partial y_j} \frac{\partial \Psi_{(j)}}{\partial y_{(i)}} \rangle_V$	$i = 2, j = 3$	$i = 1, j = 3$	$i = 1, j = 2$
	7.28×10^{-3}	7.93×10^{-3}	6.59×10^{-3}
$\langle \frac{\partial \Psi_i}{\partial y_j} \frac{\partial \Psi_m}{\partial y_n} \rangle_V$			
	-7.0×10^{-7}	-4.6×10^{-7}	5.0×10^{-7}
$ijmn = 1213$		$ijmn = 1223$	$ijmn = 2313$
5.0×10^{-7}		-8.3×10^{-7}	1.2×10^{-7}
$ijmn = 1231$		$ijmn = 1232$	$ijmn = 2331$
2.8×10^{-7}		3.3×10^{-7}	7.7×10^{-7}
$ijmn = 2113$		$ijmn = 2123$	$ijmn = 3213$
1.8×10^{-7}		-2.5×10^{-7}	-5.1×10^{-7}
$ijmn = 2131$		$ijmn = 2132$	$ijmn = 3231$

out that based on Eq. (48) and the values of \mathcal{Q} , the low Reynolds number spectrum E_1 corresponds to $O(\text{Re}_L) \approx 20$. Hence, it is expected that the present method using spectrum E_1 to generate an inhomogeneous turbulence field with a moderate spatial variation (e.g. $C_g < 1$ in Eq. (64)) would yield an error in the velocity correlation less than 5%, according to Eq. (65).

It is shown that there is only minor difference between the result from the 2nd and 4th order schemes for the curl operator; therefore, in the remaining studies only the 2nd order scheme is used.

By setting $\varphi^R = 0.315\pi$ it is seen that $\langle \frac{\partial \Psi_i}{\partial y_j} \frac{\partial \Psi_{(j)}}{\partial y_{(i)}} \rangle_V$ tends to zero with both spectra (all components are less than 0.01). It is also shown that all components of $\langle \frac{\partial \Psi_i}{\partial y_j}^2 \rangle_V$ are approximately $0.5U'^2$ when $i \neq j$, as a consequence of Eq. (50) in Lemma 1. The slightly lower value of $\langle \frac{\partial \Psi_i}{\partial y_j}^2 \rangle_V$ for E_2 (around 0.479) is related to the previously observed lower diagonal $\langle v_i v_j \rangle_V$ value for E_2 .

4.2. Inhomogeneous turbulence

4.2.1. Turbulence confined by a “slip-wall” box

In this test case a scaling function with variation in all three directions is given as:

$$c_i(x_1, x_2, x_3) = c_i(x_i) = 0.05 + \sin(\pi x_i / D_{(i)}^X), \quad (69)$$

it mimics a fictitious condition of turbulence confined inside a cubic box made of “slip-wall” at all boundaries. The size of the cubic domain is $D_i^X = 4$ m along all directions. The integral scale is set to $L = 0.5$ m and spectrum E_1 is considered.

Since c_i is a function of x_i , the coordinate transformation function can be simply set as $\tilde{c}_i(x_i) = c_i(x_i)$, which results in the \mathbf{y} -domain as a cube of size $D_i^Y = 9.2$ m. Fig. 4 shows the flow field generated from a single realization using the present

Table 2

Spatially-averaged statistical quantities of $\langle v_i v_j \rangle$, $\langle \Psi_i \Psi_j \rangle$, $\langle \frac{\partial \Psi_i}{\partial y_j} \Psi_k \rangle$, $\langle \frac{\partial \Psi_i}{\partial y_j}^2 \rangle$ and $\langle \frac{\partial \Psi_i}{\partial y_j} \frac{\partial \Psi_{(j)}}{\partial y_{(i)}} \rangle$ (respective unit: $m^2 s^{-2}$, $m^4 s^{-2}$, $m^3 s^{-2}$, $m^2 s^{-2}$ for the rest) computed from 1000 randomly generated homogeneous/isotropic turbulence fields using spectrum E_2 at $Re_L = 100$ and the 2nd order central difference scheme.

$\langle v_i v_j \rangle_V$	$j = 1$	$j = 2$	$j = 3$
$i = 1$	0.945	-8.07×10^{-5}	-2.71×10^{-5}
$i = 2$	-8.07×10^{-5}	0.945	-2.62×10^{-3}
$i = 3$	-2.71×10^{-5}	-2.62×10^{-3}	0.945
$\langle \Psi_i \Psi_j \rangle_V$	$j = 1$	$j = 2$	$j = 3$
$i = 1$	1.20×10^{-2}	-4.11×10^{-5}	-1.62×10^{-5}
$i = 2$	-4.11×10^{-5}	1.20×10^{-2}	-3.22×10^{-5}
$i = 3$	-1.62×10^{-5}	-3.22×10^{-5}	1.20×10^{-2}
$\langle \frac{\partial \Psi_i}{\partial y_j} \Psi_k \rangle_V$	$j = 1$	$j = 2$	$j = 3$
$i = 1, k = 1$	-9.7×10^{-23}	-2.3×10^{-18}	9.2×10^{-20}
$i = 2, k = 1$	-5.6×10^{-19}	-3.2×10^{-22}	-3.8×10^{-18}
$i = 3, k = 1$	-3.8×10^{-18}	-3.6×10^{-18}	-3.0×10^{-22}
$i = 1, k = 2$	-4.0×10^{-20}	-2.2×10^{-18}	-4.0×10^{-18}
$i = 2, k = 2$	3.7×10^{-19}	2.4×10^{-20}	6.7×10^{-18}
$i = 3, k = 2$	-1.7×10^{-19}	4.3×10^{-19}	-9.9×10^{-21}
$i = 1, k = 3$	-3.7×10^{-18}	4.9×10^{-18}	-5.2×10^{-18}
$i = 2, k = 3$	-1.9×10^{-18}	4.2×10^{-19}	-1.6×10^{-18}
$i = 3, k = 3$	-6.1×10^{-18}	1.5×10^{-18}	1.0×10^{-18}
$\langle \frac{\partial \Psi_i}{\partial y_j}^2 \rangle_V$	$j = 1$	$j = 2$	$j = 3$
$i = 1$	x	0.4798	0.4799
$i = 2$	0.4795	x	0.4801
$i = 3$	0.4799	0.4797	x
$\langle \frac{\partial \Psi_i}{\partial y_j} \frac{\partial \Psi_{(j)}}{\partial y_{(i)}} \rangle_V$	$i = 2, j = 3$	$i = 1, j = 3$	$i = 1, j = 2$
	7.43×10^{-3}	7.37×10^{-3}	7.21×10^{-3}

Table 3

The diagonal terms of spatially-averaged $\langle v_i v_j \rangle$ and $\langle \Psi_i \Psi_j \rangle$ (respective unit: $m^2 s^{-2}$, $m^4 s^{-2}$) computed from 1000 randomly generated homogeneous/isotropic turbulence fields with both spectra E_1 and E_2 using the 4th order central difference scheme.

E_1	$i = 1$	$i = 2$	$i = 3$
$\langle v_i v_{(i)} \rangle_V$	0.999	0.999	0.999
$\langle \Psi_i \Psi_{(i)} \rangle_V$	4.97×10^{-2}	4.95×10^{-2}	4.96×10^{-2}
E_2	$i = 1$	$i = 2$	$i = 3$
$\langle v_i v_{(i)} \rangle_V$	0.985	0.985	0.985
$\langle \Psi_i \Psi_{(i)} \rangle_V$	1.16×10^{-2}	1.16×10^{-2}	1.16×10^{-2}

method and Smirnov's method. The three velocity components from the two methods fluctuate at similar magnitudes. The new method shows that the fluctuation of j -velocity component is inhibited when approaching the j -normal boundary (e.g. the fluctuation of v_3 is suppressed near the top and bottom boundaries), whereas fluctuations in the parallel components remain unsuppressed. The flow structures near the boundary are stretched along the parallel directions, with the results from Smirnov's method showing greater and asymmetric stretching. The discrepancy is attributed to the use of \tilde{k}_j^n replacing k_j^n in Smirnov's method yields an equivalent "coordinate transformation" as $y_i(x_i) = x_i/c_{(i)}(x_i)$. Although $c_i(x_i)$ is a symmetric function with respect to the center of the domain, the Jacobian in Smirnov's method, $\partial y_i/\partial x_{(i)} = c_i^{-1} - x_{(i)} c_{(i)}^{-2} \partial c_i/\partial x_{(i)}$, is not a symmetric function. As a result, flow structures are stretched rather differently near different boundaries. In the new method, with Eq. (14), the Jacobian of the transformation, $\partial y_i/\partial x_{(i)} = c_i^{-1}$, is symmetric, which enables more "realistic" (symmetric) flow structures.

The non-symmetrical stretching pattern in the fluctuating flow structures from Smirnov's method is an unwanted artifact. A similar pattern can also be observed in the plot of the divergence error in Fig. 5. It appears that larger ε_{div} values are found near the boundary region where the spatial variation of c_i is large. With the new method divergence-free is strictly satisfied.

Fig. 6 shows the spatial distribution of the $\langle v_i v_j \rangle$ components computed using the new method. It can be seen that an i -diagonal component ($\langle v_i v_{(i)} \rangle$) varies mainly in the i -direction, with the peak values located around the center of the domain, while the off-diagonal components fluctuate around zero with a smaller magnitude, less than 0.1. A comparison of the $\langle v_i v_j \rangle$ profiles with the exact solution ($U'^2 c_i^2 \delta_{ij}$) is shown in Fig. 7, where it is seen that the agreement between the numerical results from the new method and the exact solution is good.

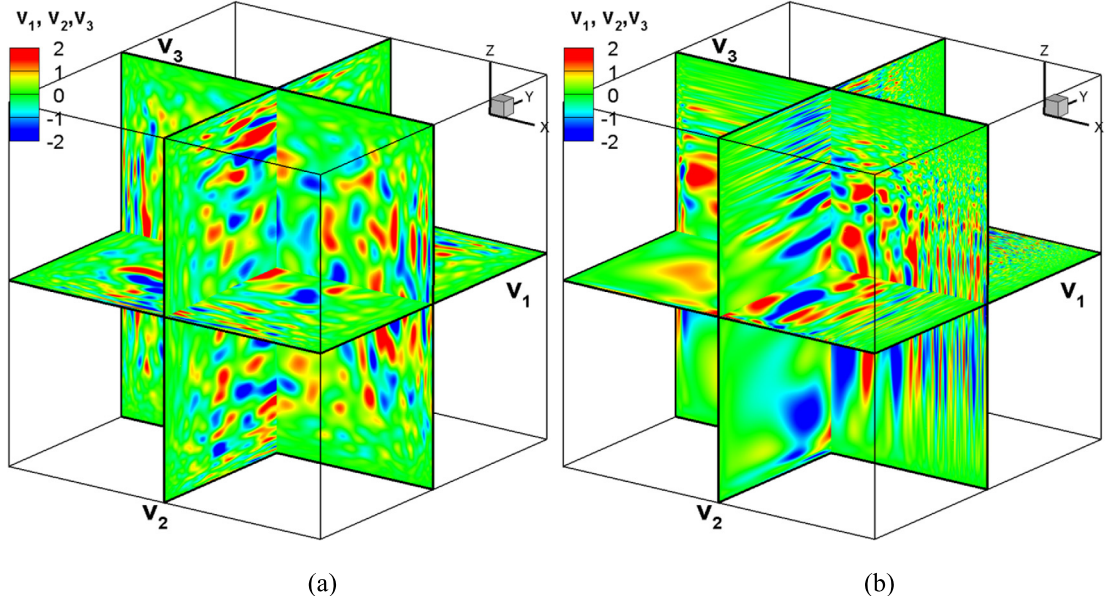


Fig. 4. Comparison of the velocity field generated from a single realization of the new method (a) and Smirnov's method (b) for the case of “slip-wall box” turbulence. E_1 spectrum is used.

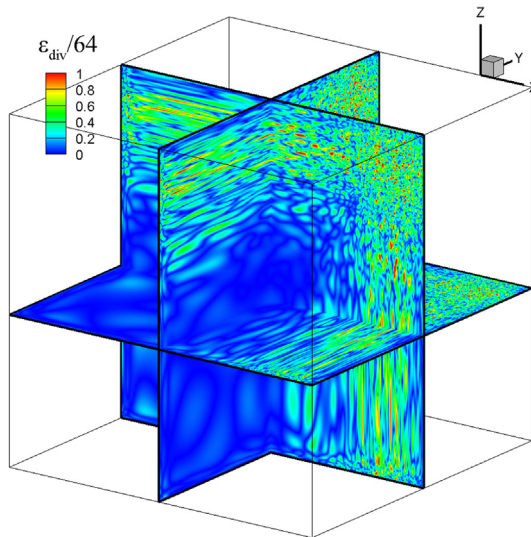


Fig. 5. The absolute divergence error (ε_{div} , unit: s^{-1}) in the flow field generated by Smirnov's method for the case of “slip-wall box” turbulence. (Same field as Fig. 4(b).)

4.2.2. Planar channel flow

In the planar channel flow case x_2 is assumed to be the wall-normal direction, whereas x_1 and x_3 are the streamwise and spanwise directions, respectively. The scaling is along the wall-normal direction x_2 ,

$$c_i(x_1, x_2, x_3) = d_i \cdot \cos(\pi/2(2x_2/D_2^X - 1)^2), \quad (70)$$

with $d_1 = 5d_2 = d_3 = 1$. The domain is set as $D_1^X = 2D_2^X = D_3^X = 4$ m. In this case we examine the generation of inhomogeneous turbulence in a non-slip wall bounded channel flow. The integral scale is assumed to be $L = 1$ m with spectrum E_1 , and $L = 4$ m with spectrum E_2 .

The coordinate transformation functions \bar{c}_i are assumed to be constants: $\bar{c}_1 = 5\bar{c}_2 = \bar{c}_3 = 1$, which leads to the domain size of $D_1^Y = 0.4D_2^Y = D_3^Y = 4$ m. It should be mentioned that although c_2 in Eq. (70) is only a function in x_2 , choosing $\bar{c}_2 = c_2$ can result in violation of criterion (34) at certain locations.

Fig. 8 shows the instantaneous velocity fields generated using the new method and Smirnov's method with spectra E_1 and E_2 . With the prescribed profile of c_i the magnitude of the v_2 component is about 1/5 of the other two components.

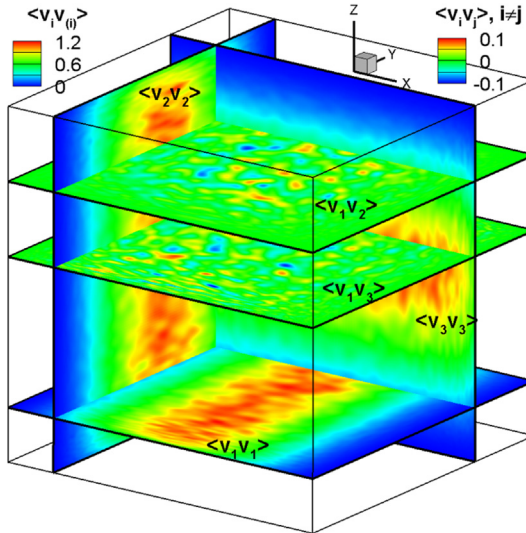


Fig. 6. Spatial distribution of $\langle v_i v_j \rangle$ in various cross sections of the domain computed using the new method with the E_1 spectrum for the case of “slip-wall box” turbulence. $\langle v_i v_j \rangle$ is averaged from 1000 realizations.

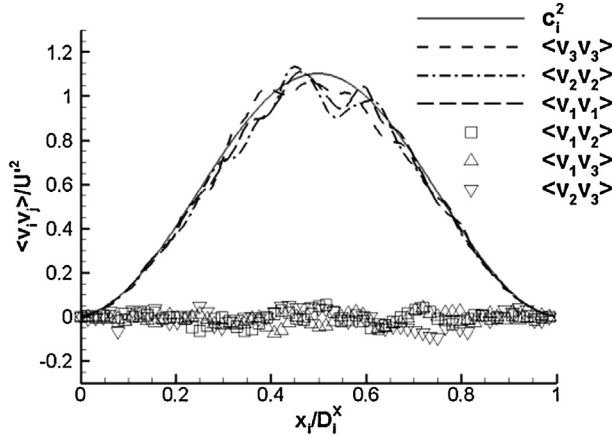


Fig. 7. A comparison between $\langle v_i v_j \rangle$ computed using the new method with the E_1 spectrum and the exact solution for the case of “slip-wall box” turbulence. $\langle v_i v_j \rangle$ is averaged from 1000 realizations.

While being rather homogeneous along the x_1 and x_3 directions, the velocity fluctuation is found to be inhibited near the two walls in the x_2 -direction. With the high Reynolds number spectrum E_2 , the flow field exhibits much richer scales than the fields with the E_1 spectrum. Similar to the previous test cases the flow field generated from Smirnov’s method shows a non-symmetrical stretching of flow structures, which appears stronger in the region near the upper wall (y -direction shown in the figure). The new method produces rather symmetrical structures when approaching the walls with both spectra. The stretching in the flow structures is also less pronounced than that in the previous example. This is because \bar{c}_i is constant in the present case whereas c_i varies in space in the previous case.

Fig. 9 shows the divergence error in the results from Smirnov’s method. A large divergence error can be found near the top and bottom walls where a large gradient in c_i exists.

The velocity correlation tensor computed using the new method is shown in Fig. 10. The spatial distribution of diagonal terms corresponds well to the given scaling function (only varying in x_2), while the off-diagonal fluctuations are small. A quantitative comparison is shown in Fig. 11 where the prescribed scaling function is plotted together with the computed correlation components along the x_2 -direction through the domain center. Except certain scattering caused by insufficient sampling, the diagonal components match the prescribed scaling functions rather well. The off-diagonal components are small.

4.2.3. Annular flow

In this example the scaling function is given to mimic turbulent annular flow as (x_1 is the axial direction),

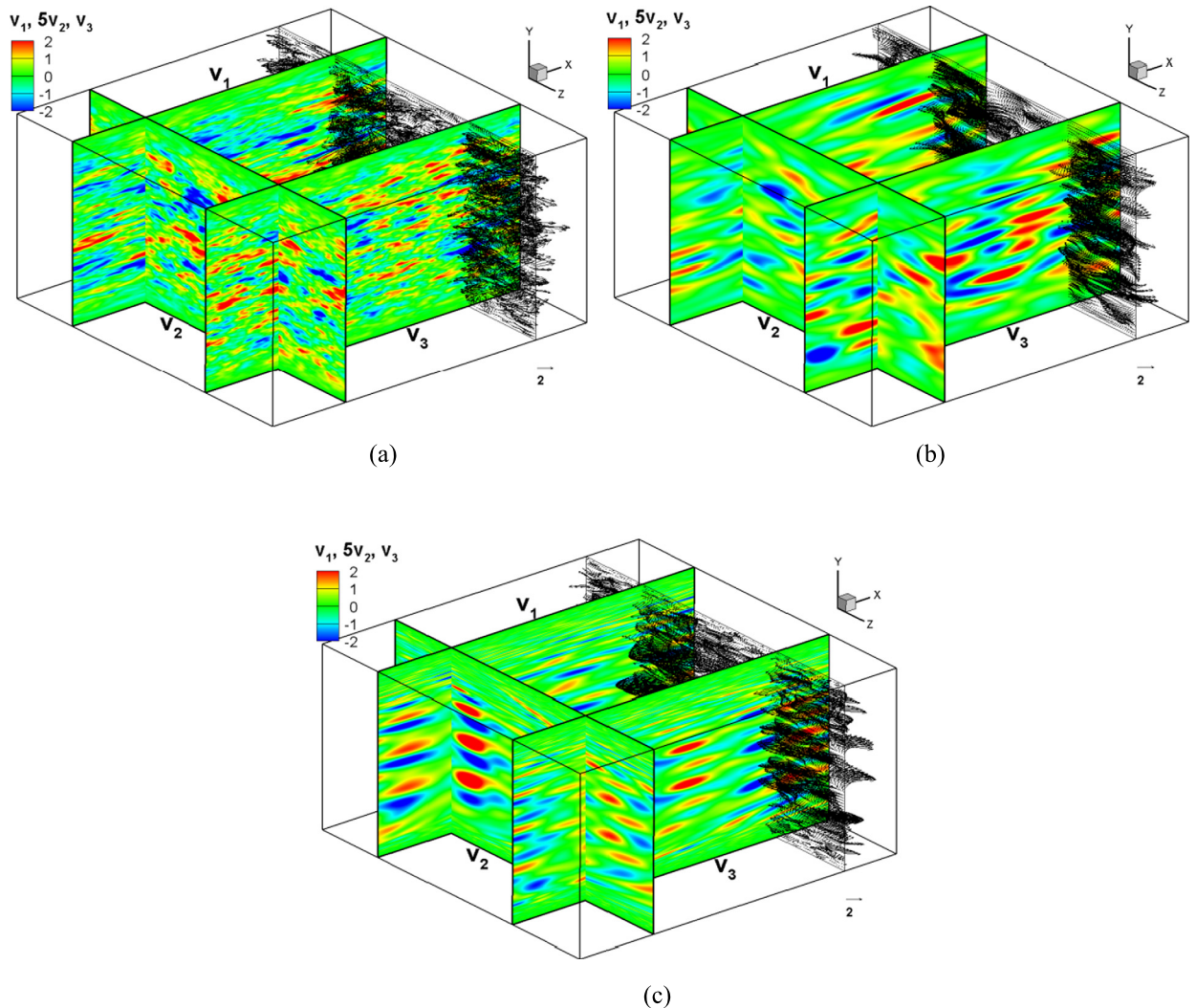


Fig. 8. Comparison of the instantaneous velocity field generated from a single realization of the new method with spectrum E_2 (a), E_1 (b), and Smirnov's method with E_1 (c), for the planar channel flow case.

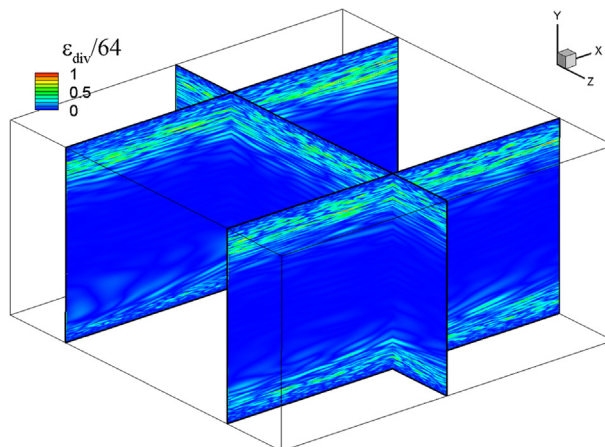


Fig. 9. The absolute divergence error (ϵ_{div} , unit: s^{-1}) in the flow field generated with Smirnov's method for the planar channel flow case. (Same field as Fig. 8(b).)

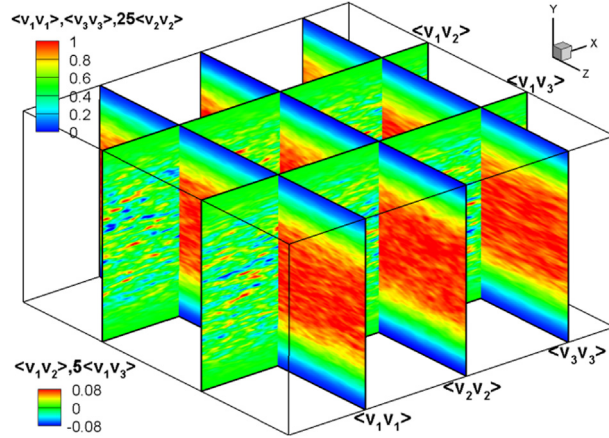


Fig. 10. Distributions of $\langle v_i v_j \rangle$ for the planar channel flow case. $\langle v_i v_j \rangle$ is averaged from 1000 realizations with the new method and the E_2 spectrum at $Re_L = 100$.

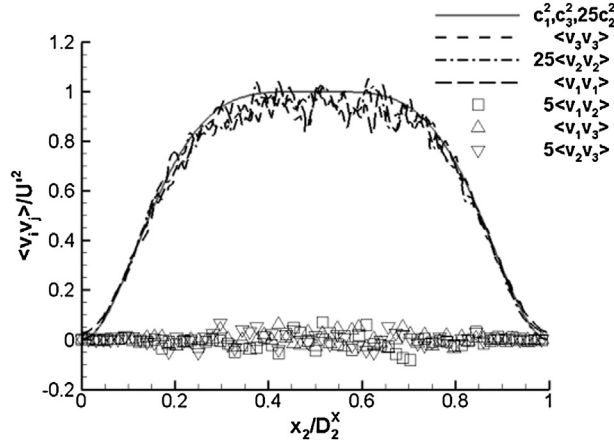


Fig. 11. A comparison of the prescribed c_i^2 profile with the computed $\langle v_i v_j \rangle$ components for the planar channel flow case. $\langle v_i v_j \rangle$ is averaged from 1000 realizations with the new method and the E_2 spectrum at $Re_L = 100$. All the $\langle v_i v_j \rangle$ components are plotted along the x_2 -direction through the domain center.

$$c_i(x_1, x_2, x_3) = \begin{cases} \sin(r)b_i & r \in [0, \pi], \\ 0 & r \notin [0, \pi], \end{cases} \quad (71)$$

with

$$r(x_1, x_2, x_3) = 3\pi \sqrt{(x_2/D_2^X - 1/2)^2 + (x_3/D_3^X - 1/2)^2} - 0.4\pi, \quad (72)$$

and $b_1 = 5b_2 = 5b_3 = 1$. The domain is set as $D_1^X = D_2^X = D_3^X = 4$ m. The integral scale is set to $L = 1$ m and the spectrum E_1 is used.

The coordinate transformation functions are set as constants, $4\bar{c}_1 = \bar{c}_2 = \bar{c}_3 = 1$, which yields a y -domain size as $D_1^Y = D_2^Y = D_3^Y = 4$ m.

Fig. 12 shows the velocity fields from the new method and the Smirnov method with the spectrum E_1 . Both methods produce comparable levels of velocity fluctuations to those observed in previous cases. It is obvious, however, that the Smirnov method creates an unphysical pattern of spirally stretched structures on the axial cutting plane, with a large divergence error, shown in Fig. 13. This pattern is again a consequence of Smirnov's method of "coordinate transformation". The proposed new method generates more physical fluctuating structures that are strictly divergence-free.

Fig. 13 shows the divergence error (ϵ_{div}) in the results obtained using the Smirnov method. Larger divergence errors are found around two ring band regions in between the center radius and the inner/outer radii, where both the values of \mathbf{c} and \mathbf{c} -gradient are not negligible.

The velocity correlation tensor computed with the present new method is shown in Fig. 14. It is clear that the diagonal terms agree well with the prescribed profile of c_i^2 as shown in the x_2 - x_3 plane (y - z plane in the figure), while the off-diagonal components' fluctuation is negligible. Fig. 15 shows the components of the tensor along the x_2 -direction through

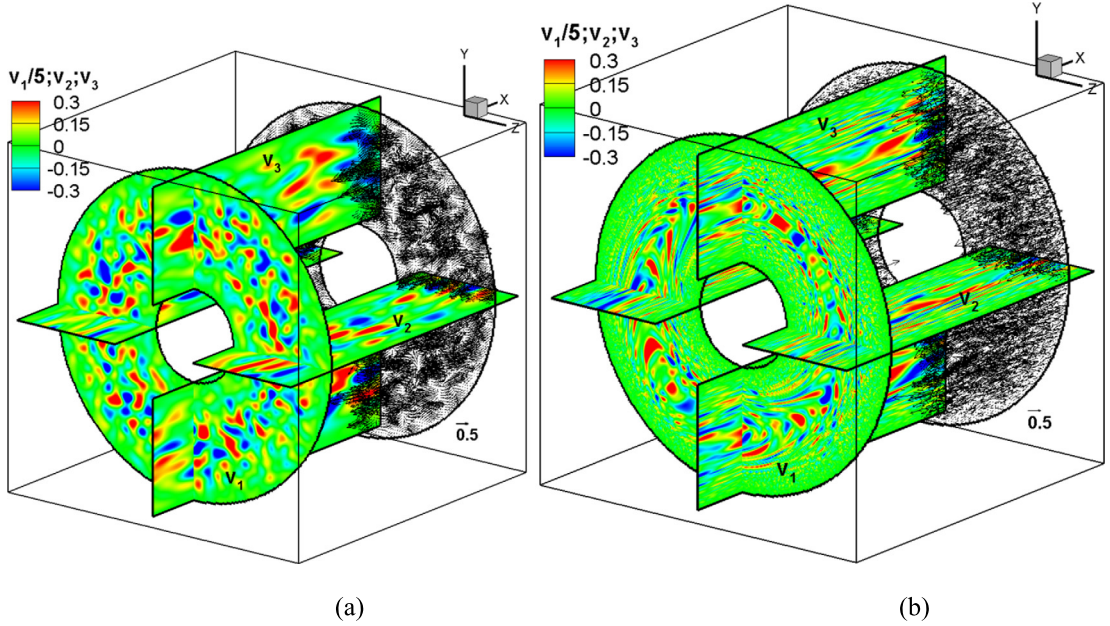


Fig. 12. Velocity fields generated from single realization of the new method (a) and Smirnov's method (b) for the annular flow case. The E_1 spectrum is used.

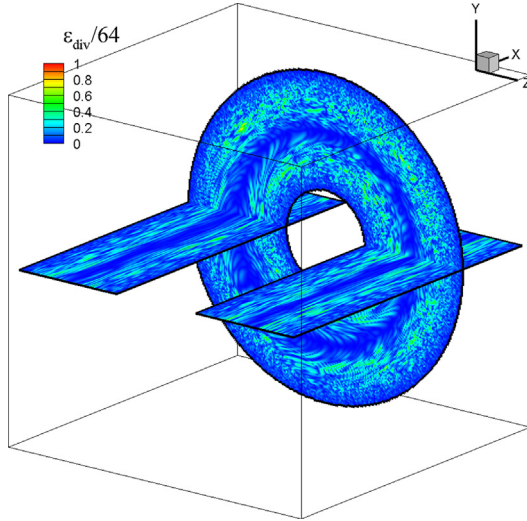


Fig. 13. The absolute divergence error (ε_{div} , unit: s^{-1}) in the flow field generated with Smirnov's method for the annular flow case. (Same field as Fig. 12(b).)

the domain center. Again, the off-diagonal terms can be neglected and the diagonal components fit well to the prescribed c_i^2 profile.

5. Summary and conclusion

A new method is proposed for generating a general, fully divergence-free inflow/initial-flow field for inhomogeneous turbulence with large spatial variation. The method is based on the widely used method of Smirnov et al. for inhomogeneous/anisotropic turbulence, in which violation of divergence-free constraint becomes non-negligible under conditions with significant spatial variation. The proposed method is based on Smirnov's framework consisting of a scaling step and an orthogonal transformation step.

The new method is based on the idea that any divergence-free velocity field can be obtained from the curl of a vector potential field. In the new method a vector potential field for homogeneous/isotropic turbulence is generated. It is then modified using a novel scaling formulation together with a coordinate transformation strategy. We propose to perform the

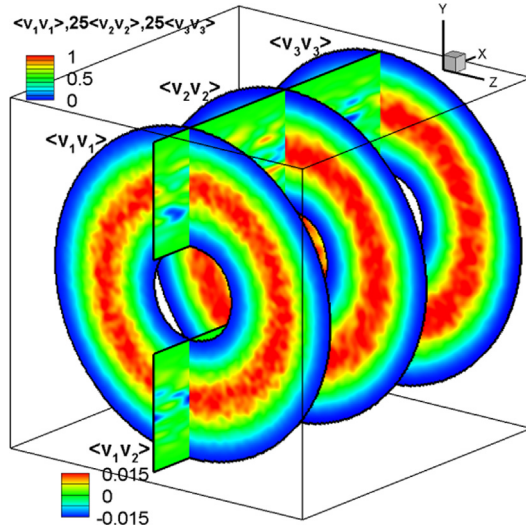


Fig. 14. Distribution of $\langle v_i v_j \rangle$ for the annular flow case. $\langle v_i v_j \rangle$ is averaged from 1000 realizations using the new method and spectrum E_1 .

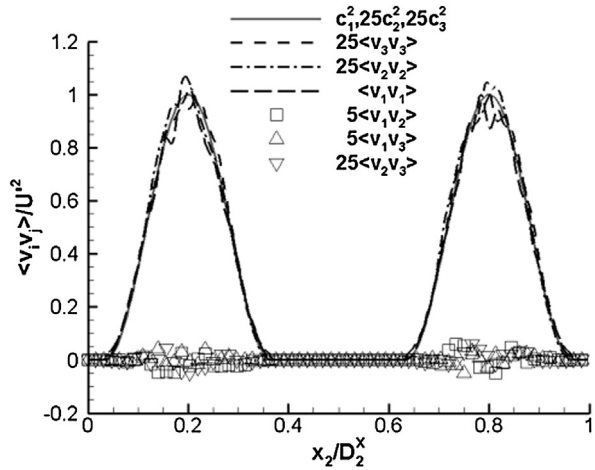


Fig. 15. A comparison of the prescribed c_i^2 profile with the computed $\langle v_i v_j \rangle$ components for the annular flow case. $\langle v_i v_j \rangle$ is averaged from 1000 random realizations using the new method and spectrum E_1 . All $\langle v_i v_j \rangle$ components are plotted along the x_2 -direction through the domain center.

scaling on the vector potential field, instead of on the velocity field. The final velocity, after taking the curl of the modified vector potential, is then always divergence-free.

A proof is given to show that the proposed scaling formulation for modifying the homogeneous vector potential is able to reproduce the prescribed scaled velocity correlation under strong spatial variation at reasonably large Reynolds numbers.

The new method is first demonstrated in a homogeneous turbulence case, in which the homogeneous vector potential and velocity fields are compared with two energy spectra: one with a high and the other with a low Reynolds number. The higher order statistics computed with both ensemble and spatial averaging verify the formulations. This is essential for the error estimation of the proposed method when applied to inhomogeneous conditions.

We then applied the new method to three inhomogeneous turbulence cases with different scaling functions: a fictitious turbulence confined by a “slip-wall” box, a turbulent planar channel flow and a turbulent annular flow. These cases represent theoretical flows and practical applications when the inflow/initial-flow conditions are needed. In these cases various choices of coordinate transformation are demonstrated. In each case the flow field from the proposed method is compared with the one given by Smirnov’s method. It is seen that unphysically stretched flow structures found in the results from the Smirnov method can be removed with the new method. The advantage of the new method is highlighted by showing the different divergence-error distribution from the Smirnov method; an error which is absent in the new method. Furthermore, the field of the velocity correlation tensor calculated from ensemble averaging of multiple realizations from the new method are shown to agree well with the given scaling functions.

Compared with the previously suggested method of using an extra projection step to remove the divergence error – which complicates the algorithm and introduces an undefined deviation from the given statistics, the proposed method is

simple to implement and deviations from prescribed velocity correlation are small. The computational efficiency of the new method is nearly the same as the original Smirnov method.

Acknowledgements

This work is supported by the Swedish Research Council (VR), and partly sponsored by the Swedish National Center for Combustion Science and Technology (CeCOST). We acknowledge PRACE for awarding us access to resource CURIE based in France at the Très Grand Centre de Calcul (TGCC).

References

- [1] L. Davidson, M. Billson, Hybrid LES-RANS using synthesized turbulent fluctuations for forcing in the interface region, *Int. J. Heat Fluid Flow* 27 (2006) 1028–1042.
- [2] M. Pamies, P.E. Weiss, E. Garnier, S. Deck, P. Sagaut, Generation of synthetic turbulent inflow data for large eddy simulation of spatially evolving wall-bounded flows, *Phys. Fluids* 21 (2009) 045103.
- [3] A. Keating, U. Piomelli, E. Balaras, H.J. Kaltenbach, A priori and a posteriori tests of inflow conditions for large-eddy simulation, *Phys. Fluids* 16 (2004) 4696–4712.
- [4] G.R. Tabor, M.H. Baba-Ahmadi, Inlet conditions for large eddy simulation: A review, *Comput. Fluids* 39 (2010) 553–567.
- [5] R.H. Kraichnan, Diffusion by a random velocity field, *Phys. Fluids* 13 (1970) 22.
- [6] A. Smirnov, S. Shi, I. Celik, Random flow generation technique for Large Eddy Simulations and particle-dynamics modeling, *J. Fluids Eng. Trans. ASME* 123 (2001) 359–371.
- [7] M. Klein, A. Sadiki, J. Janicka, A digital filter based generation of inflow data for spatially developing direct numerical or large eddy simulations, *J. Comput. Phys.* 186 (2003) 652–665.
- [8] A. Kempf, M. Klein, J. Janicka, Efficient generation of initial- and inflow-conditions for transient turbulent flows in arbitrary geometries, *Flow Turbul. Combust.* 74 (2005) 67–84.
- [9] Z.T. Xie, I.P. Castro, Efficient generation of inflow conditions for large eddy simulation of street-scale flows, *Flow Turbul. Combust.* 81 (2008) 449–470.
- [10] N. Jarrin, S. Benhamadouche, D. Laurence, R. Prosser, A synthetic-eddy-method for generating inflow conditions for large-eddy simulations, *Int. J. Heat Fluid Flow* 27 (2006) 585–593.
- [11] P. Batten, U. Goldberg, S. Chakravarthy, Interfacing statistical turbulence closures with large-eddy simulation, *AIAA J.* 42 (2004) 485–492.
- [12] R. Poletto, A. Revell, T. Craft, N. Jarrin, Divergence free synthetic eddy method for embedded LES inflow boundary conditions, in: Seventh International Symposium on Turbulence and Shear Flow Phenomena (TSFP-7), Ottawa, 2011.
- [13] S.H. Huang, Q. Li, J.R. Wu, A general inflow turbulence generator for large eddy simulation, *J. Wind Eng. Ind. Aerodyn.* 98 (2010) 600–617.
- [14] S.B. Pope, *Turbulent Flows*, Cambridge University Press, Cambridge, New York, 2000.